Singularity-Free Approximate Waypoint Tracking Controller for Underactuated Magnetic Robots

Suraj Raval * **Anuruddha Bhattacharjee** ** **Xinhao Chen** **
Lamar Mair *** **Axel Krieger** ** **Yancy Diaz-Mercado** *

* *Mechanical Engineering Department, University of Maryland, College Park, MD 20742 USA (e-mail: sraval@umd.edu, yancy@umd.edu).*
** *Laboratory for Computational Sensing and Robotics, Johns Hopkins University, Baltimore, MD 21218, USA (e-mail: abhatt27@jhu.edu, xchen254@jhu.edu, axel@jhu.edu)*
*** *Division of Magnetic Manipulation and Particle Research, Weinberg Medical Physics, Inc., North Bethesda, MD 20852 USA (e-mail: lamar.mair@gmail.com)*

Abstract: Magnetic robots use external magnetic fields to draw energy, generating steering capabilities crucial for minimally invasive surgeries and enabling next generation untethered surgical tool miniaturization. However, accurate control is challenging due to configuration-dependent singularities in the manipulation Jacobian, which can cause unsafe behavior with standard controls. We analyze the nonlinear nature of magnetic fields to understand singularity-free control limits without adding more magnetic actuators, which increases bulk and cost. Using Chow's Theorem, we study the motion feasibility of a single magnetic robot moving in a plane, powered by stationary electromagnets. We determine the degree of nonholonomy for an underactuated case and show that any desired motion in the state-space can be approximated with more complex controls. We deploy an approximate-tracking controller to steer a magnetic robot between any two points in the state-space, avoiding singularities. Simulations show a 0.82 mm RMS positional tracking error for an 8 mm long cylindrical magnetic tool using our method.

Keywords: Magnetic Robots, Nonlinear Control Systems, Robotics, Path Planning and Motion Control, Robot Manipulators

1. INTRODUCTION

Modeling, estimation, and precision control of robotic manipulators are crucial for robot-assisted surgery. Recent studies (Saeidi et al. (2022); Kuntz et al. (2023)) show increased procedure success rates and reduced human errors with surgical robots. Additional benefits include decreased tissue trauma, faster patient recovery, and improved patient satisfaction (Maeso et al. (2010)). State-of-the-art surgical robots like the Da Vinci Surgical System utilize mechanical manipulators for precise motion control. While minimally invasive surgeries through a single incision (Antoniou et al. (2011)) or natural orifices (Chamberlain and Sakpal (2009)) have enhanced outcomes, the bulkiness of mechanical manipulators limits the range of procedures possible due to the physical connection between the end effector and the actuator.

Untethered robotic tools guided by external magnetic fields can enhance access and reach for surgical instruments, facilitating procedures deep inside the patient's body where maneuverability is crucial (Wang et al. (2022); Dreyfus et al. (2024)). Various magnetic tools, such as catheter (Dreyfus et al. (2024)), cutting tool (Bao and Diller (2022)), needle (Erin et al. (2022a)), and grippers (Zhang et al. (2017)), can be manipulated by the application of magnetic forces and torques from the external magnetic field generated by electromagnetic coils. A few examples of sophisticated electromagnetic systems include OctoMag (Kummer et al. (2010)), BatMag (Ongaro et al. (2018)), and MagnetoSuture (Mair et al. (2020)).

A major challenge in implementing magnetic robots in clinical settings is their controllability. Underactuated magnetic actuation systems experience state-dependent singularities, complicating motion control (Petruska and Nelson (2015a); Erin et al. (2022b)). Near these singularities, the actuation matrix becomes ill-conditioned, causing standard controllers to struggle with sudden spikes in control inputs, leading to reduced control effectiveness and potential instability. Depending on the coil array configuration, the state-space includes multiple points where the robot can encounter these singularities, preventing simultaneous achievement of desired forces and torques to meet control objectives.

In magnetic robotics, feedback linearization techniques (Abbott et al. (2020); Raval et al. (2021)) are common and effective with accurate models, unless the actuation matrix becomes singular. Methods like Tikhonov regularization (Zhao et al. (2020)) and regularization-based singular value decomposition (Nguyen et al. (2020)) aim to address

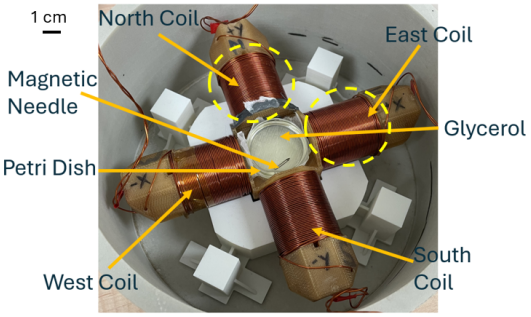

Fig. 1. Magnetic system with the circled coils used for this paper. Each coil has 29 turns with 14 layers. Coil radius and length are 15.5 and 40.5 mm respectively.

these issues, primarily focusing on position control rather than simultaneous heading and position control. Some approaches (Salehizadeh and Diller (2021); Fruchard (2023)) have used nonlinear analysis for path planning and control of multiple magnetic tools but ignored the singularities arising from generating coil currents for desired forces and torques. Due to the nonlinear field dynamics, we use nonlinear analysis to assess motion feasibility for a single magnetic robot moving in a plane, synthesizing piecewise constant input controller to achieve feasible motion around singular configurations. The controller is used to achieve approximate tracking of a reference path, which is generated without explicit consideration of singularities in the space.

The paper is organized as follows: Section 2 covers the fundamental equations for magnetic actuation. Section 3 introduces nonlinear controllability analysis for magnetic systems. An approximate singularity-free tracking controller is given in Section 4. Simulation results are given in Section 5. Section 6 offers concluding remarks.

2. PROBLEM FORMULATION

2.1 Magnetic System Description

We consider the motion of a magnetic tool in a plane achieved by application of an external magnetic field generated by an array of stationary electromagnetic coils surrounding the workspace. The coils' magnetization axes intersect at the workspace center. The magnetic tool, a rigid body with permanent magnetization (1.41 T Remanence), has three degrees of freedom: translation and rotation in the plane. Fig. 1 shows such a system with four coils around a 37 mm diameter circular workspace, powered by RoboClaw motor controllers with an Arduino interface. An overhead camera facilitates magnetic tool tracking. Since this paper focuses on control of underactuated magnetic systems, while we assume any number of coils are available in subsequent analysis, we limit control to two (east and north) of the four coils.

2.2 Actuation Forces and Torques

Let the magnetic tool workspace (37 mm diameter petri dish) be $\mathcal{W} \subset \mathbb{R}^2$. Let $x \in W$ be the center of mass position of a rigid magnetic tool. The magnetic tool has permanent magnetization which is uniformly distributed over the rigid body. The north axis of magnetization is parameterized by the orientation angle $\theta \in [0, 2\pi]$. The magnetization vector $M(\theta) \in \mathbb{R}^2$ indicates the tool heading such that $\frac{M}{\|M\|} = [\cos\theta \quad \sin\theta]^T$ with constant $\|M\| > 0$. The torque $\tau \in \mathbb{R}$ and force $F \in \mathbb{R}^2$ generated by an external magnetic field vector at the tool location, $B(x) \in \mathbb{R}^2$, is given by

$$\tau = M(\theta)^T S B(x), \quad S = \begin{bmatrix} 0 & -1 \\ 1 & 0 \end{bmatrix}, \quad F = \nabla B(x) M \tag{1}$$

where the gradient $\nabla B \in \mathbb{R}^{2\times 2}$ is symmetric due to magnetic field properties (Petruska and Nelson (2015b)).

The external magnetic field is generated by the superposition of the magnetic field generated by m electromagnets. Let $u_k \in \mathbb{R}$ be the controllable current applied to the k^{th} electromagnetic coil. By the Biot-Savart law, the magnetic field generated by each coil is proportional to the applied current, so the external magnetic field is given by

$$B(x) = \sum_{k=1}^{m} \bar{B}_k(x) u_k \tag{2}$$

where $\bar{B}_k(x) \in \mathbb{R}^2$ is a position-dependent vector field for k^{th} coil.

As done in Salehizadeh and Diller (2016), Raval et al. (2023), we assume first-order dynamics of the form

$$\dot{x} = \tfrac{1}{c_t} F = \tfrac{1}{c_t} \sum_{k=1}^{m} \nabla \bar{B}_k(x) M(\theta) u_k \tag{3}$$

$$\dot{\theta} = \tfrac{1}{c_r} \tau = \tfrac{1}{c_r} \sum_{k=1}^{m} M(\theta)^T S \bar{B}_k(x) u_k \tag{4}$$

for damping coefficients c_t (5.14×10^{-2} N.s/m), c_r (4×10^{-7} N.s.m/rad). The vector field $\bar{B}_k$ depends on the geometry of the electromagnetic coils and accurate representations are numerically costly. For this reason, these vector fields are commonly approximated using dipole model (see Appendix A), which provides a closed-form solution. Let $X = [x^T, \theta]^T \in \mathbb{R}^3$, then the magnetic tool dynamics are given by the driftless control affine system

$$\dot{X} = \sum_{k=1}^{m} g_k(X) u_k \tag{5}$$

where the vector fields $g_k : \mathbb{R}^3 \to \mathbb{R}^3$ map any point in the state-space to the corresponding state velocities (proportional to forces and torques generated by the k^{th} coil), given by

$$g_k(X) = \begin{bmatrix} \frac{1}{c_t} \nabla \bar{B}_k(x) M(\theta) \\ \frac{1}{c_r} M(\theta)^T S \bar{B}_k(x) \end{bmatrix} \tag{6}$$

2.3 Actuation Matrix

More generally, we let $u = [u_1, \ldots, u_m]^T \in \mathbb{R}^m$ be the stacked vector of control inputs and $g \in \mathbb{R}^{n\times m} : \mathcal{X} \to \mathcal{X} \subseteq \mathbb{R}^n$ ($n = 3$ in our case) be the actuation matrix for the electromagnetic actuation system. As a result, we get

$$\dot{X} = g(X) u \tag{7}$$

This paper focuses on understanding the controllability limitations of (7) under the nonlinear nature of the actuation matrix. We use nonlinear analysis to achieve motion control that the existing feedback linearization techniques, limited by singularities in g, might have been deemed infeasible. Method details ensue.

3. NONLINEAR CONTROLLABILITY FOR MOTION FEASIBILITY OF MAGNETIC ROBOTS

Given a driftless nonlinear system as in (5), Chow's Theorem (Sastry, 2013, Ch. 11) provides two key insights: (i) Can we go from any initial to any final state within the state-space in finite time? (ii) If so, how complex must this motion be?

3.1 Lie Brackets

To apply Chow's Theorem, we first introduce the concept of Lie brackets. The Lie bracket of vector fields g_1 and g_2 is

$$[g_1, g_2] = \frac{\partial g_2}{\partial X} g_1 - \frac{\partial g_1}{\partial X} g_2 \tag{8}$$

Practically, the motion along the Lie bracket of two vector fields can be achieved in a small amount of time by an elaborate switching between the inputs corresponding to these fields (Sastry (2013). If the vector fields corresponding to the matrix $g(X)$ spans $\mathbb{R}^n$ at every point in the state-space, then we can move from any initial to any final state with the least complex motion.

If the matrix $g(X)$ does not span $\mathbb{R}^n$, it may be possible to span $\mathbb{R}^n$ with additional vector fields taken from the Lie brackets. Specifically, we let $\Delta = \text{span}\{g_1, \ldots, g_m\}$ be the distribution of the system. A *filtration* is a chain of nested distributions such that

$$F_i = F_{i-1} + [F_1, F_{i-1}], \quad F_1 = \Delta \tag{9}$$

$$[F_1, F_{i-1}] = \text{span}\{[g_1, g_2] \mid g_1 \in F_1,\ g_2 \in F_{i-1}\} \tag{10}$$

We now present Chow's theorem (Sastry, 2013, Ch. 11) for general driftless control affine systems.

Theorem 1. (Chow's Theorem). For a system as in (7), there exists admissible controls to steer the system between two arbitrary points X_0 and X_1 iff for some q

$$F_q(X) = T\mathbb{R}^n \simeq \mathbb{R}^n \quad \forall X \in \mathcal{X} \tag{11}$$

A second-order filtration would span the space of $m + p$ elements, where p the number of Philip Hall basis (Sastry (2013)) of second-order Lie brackets from the vector fields present in $g(X)$. Extending the process, we can construct higher-order filtrations from higher-order Lie brackets of vector fields. The lowest order filtration F_q that one can construct that spans $\mathbb{R}^n$ in the state-space gives us the degree of nonholonomy of the system, given by q. A higher degree of nonholonomy leads to potentially more complex motion being necessary to span the state-space.

Chow's Theorem does not provide a method to achieve this motion, but indicates its feasibility. We first apply Chow's Theorem to analyze the controllability of magnetic systems before addressing controller synthesis.

3.2 Conditions for First Filtration to be Full Rank for a General Magnetic Robotic System

For the system dynamics given in (5), the first filtration $F_1(X)$ corresponds to the vector fields in the actuation matrix $g(X)$. To establish system's controllability, given the magnetic fields' explicit structure, we first present a lemma on the rank of a square symmetric matrix.

Lemma 2. For a symmetric matrix $A \in \mathbb{R}^{n\times n}$, made up of block matrices $P \in \mathbb{R}^{m\times m}$, $Q \in \mathbb{R}^{m\times(n-m)}$, $V \in \mathbb{R}^{(n-m)\times(n-m)}$ with $m < n$, such that

$$A = \begin{bmatrix} P & Q \\ Q^T & V \end{bmatrix} \tag{12}$$

if $\text{Range}(Q) \subseteq \text{Range}(P)$, $\text{Range}(Q^T) \subseteq \text{Range}(P^T)$, then

$$rank(A) = rank(P) + rank(V - Q^T P^+ Q) \tag{13}$$

Corollary 3. A necessary condition for square symmetric matrix A to span $\mathbb{R}^n$ is that $P \in \mathbb{R}^{m\times m}$ must be full rank.

In order to determine rank of $F_1(X)$, we determine the rank of $G_1(X) = g(X)g(X)^T$, by relating it with A (12)

$$G_1(X) = \begin{bmatrix} \sum_{k=1}^{m} \nabla\bar{B}_k M M^T \nabla\bar{B}_k & \sum_{k=1}^{m} \nabla\bar{B}_k M M^T S\bar{B}_k \\ \sum_{k=1}^{m} \bar{B}_k^T S^T M M^T \nabla\bar{B}_k & \sum_{k=1}^{m} \bar{B}_k S^T M M^T S\bar{B}_k \end{bmatrix} \tag{14}$$

From Lemma 2, we can compute the rank of $F_1(X)$ in the following manner

$$rank(G_1 G_1^T) = rank(P) + rank(V - Q^T P^+ Q) \tag{15}$$

Corollary 3 suggests that we need P to be full rank for F_1 to be full rank. Since P is a summation of m matrices, each corresponding to a coil, we analyze the general matrix $\nabla\bar{B}_k M M^T \nabla\bar{B}_k \in \mathbb{R}^{2\times 2}$ corresponding to the k^{th} coil.

Lemma 4. The eigenvalues of $\nabla\bar{B}_k M M^T \nabla\bar{B}_k^T$ are

$$[\lambda_{k_1}, \lambda_{k_2}] = [0, f_{k_x}^2 + f_{k_y}^2]$$

where the eigenvector related to λ_{k_2} is $a_{k,2} = f_k/\|f_k\|$ with

$$\nabla\bar{B}_k M = f_k = \begin{bmatrix} f_{k_x} & f_{k_y} \end{bmatrix}^T \tag{16}$$

Proof. Because $\nabla\bar{B}_k M_m = f_k \in \mathbb{R}^2$, $\nabla\bar{B}_k M_m M_m^T \nabla\bar{B}_k^T = f_k f_k^T$ is a rank 1 matrix, with all eigenvalues being zero, except for one whose value is equal to $\|f_k\|^2$ with associated eigenvector $f_k/\|f_k\|$.

Corollary 5. It can be seen from Lemma 4 that

$$rank(\nabla\bar{B}_k M M^T \nabla\bar{B}_k^T) \leq 1$$

since $\lambda_{k_1} = 0$. Furthermore, if $f_{k_x}^2 + f_{k_y}^2 = 0$, then $rank(\nabla\bar{B}_k M M^T \nabla\bar{B}_k^T) = 0$. Otherwise, the rank is 1.

Now, write P as

$$P = \sum\nolimits_{k=1}^{m} \lambda_{k_2} a_{k_2} a_{k_2}^T \tag{17}$$

where, $\lambda_{k_2} = \|f_k\|^2$ is the non-zero eigenvalue for the k^{th} coil, while $a_{k_2} = f_k/\|f_k\|$ is the related eigenvector.

Theorem 6. A necessary condition for a magnetic tool to be small-time locally controllable in the workspace $\mathcal{W}$ with degree of nonholonomy 1 is for the individual $\nabla\bar{B}_k M$ to be linearly independent for at least 2 electromagnets at every point in the workspace.

Proof. To achieve small-time local controllability with degree of nonholonomy 1, per Theorem 1, we need $F_1(X)$ to be full rank. A necessary condition is that at least two of the $f_k = \nabla\bar{B}_k M$ are linearly independent, per the results of Corollary 3, Corollary 5 and (17).

Theorem 6 gives a necessary condition which requires computing magnetic field gradients and not the field itself. It is also applicable to magnetic systems with arbitrary number of coils. If this condition is not met at every point in the workspace, F_1 does not span $\mathbb{R}^n$ throughout the workspace, requiring a higher order filtration for singularity-free motion. If the condition in Theorem 6 is met, then one needs to make sure, based on Lemma 2, that $V \neq Q^T P^+ Q$ in the workspace, for $F_1(X)$ to be full rank. Meeting both conditions implies $F_1(X)$ is full rank and the system has a degree of nonholonomy of one.

3.3 Rank Conditions for Underactuated Magnetic System

We test the condition of Theorem 6 in the previous section for our magnetic system shown in Fig. 1, with only two coils (east and north) used, i.e., when $m = 2$. We can easily

verify that the vectors $\nabla \bar{B}_k M$ lose rank when the magnetic tool is located along the center axis of the k^{th} coil and is oriented perpendicular to the magnetic field. Thus, for our magnetic system workspace, we need a second-order filtration to meet Chow's Theorem conditions.

Since $F_1(X)$ does not span $\mathbb{R}^n$, we can construct the filtration $F_2(X) = \text{span}\{g_1, g_2, g_3\}$ where

$$g_3 = [g_1, g_2] = \frac{\partial g_2}{\partial X} g_1 - \frac{\partial g_1}{\partial X} g_2 \tag{18}$$

Like before, it suffices to evaluate the rank of the matrix

$$G_2(X) = \sum\nolimits_{k=1}^{3} g_k(X) g_k(X)^T \tag{19}$$

We added a vector field option ($g_3(X)$) to check for at least two linearly independent vectors at each point in the workspace. We perform a numerical search over the workspace to ensure linear independence. We discretize the state-space with a 0.1 mm spatial grid in $\mathcal{W}$ and angular resolution of 1° for $\theta \in [0, 2\pi]$. We compute the rank and condition number of $G_2(X)$ in the state-space using a dipole model (Appendix A). We find that $F_2(X)$ has full rank in the entire state-space grid. The mean condition number at the discretized points is 8.35×10^{-4} with a standard deviation of 8.75×10^{-4}. Hence, the standard deviation suggests that most points in the state-space lie within an order of magnitude of the mean reciprocal condition number. The reciprocal condition number ranges from 1×10^{-8} to 1×10^{-2}, indicating the theoretical and practical degree of nonholonomy of our particular magnetic system is two.

4. APPROXIMATE STEERING OF A MAGNETIC ROBOT WITH LIE BRACKET MOTIONS

4.1 Motion Generation with Piecewise Constant Inputs

We apply the steering algorithm from Lafferriere and Sussmann (1991) to magnetic systems. This algorithm has two steps: first, representing the system's extended dynamics with virtual inputs $v \in \mathbb{R}^{m+p}$ and computing the required virtual inputs to generate the desired trajectory. Second, generating these virtual inputs using the original system's inputs $u \in \mathbb{R}^m$. For more details, see Lafferriere and Sussmann (1991). The extended system dynamics are

$$\dot{X} = g_1(X)v_1 + \cdots + g_m(X)v_m + \cdots + g_{m+p}(X)v_{m+p} \tag{20}$$

The vector fields g_i with $i > m$ are the Lie brackets. Hence, for a desired trajectory $\gamma(t)$, we can write,

$$\dot{\gamma}(t) = \left[g_1(\gamma(t)) \ \cdots \ g_{m+p}(\gamma(t)) \right] v \tag{21}$$

where $v = [v_1, \ldots, v_{m+p}]^T$. By construction, the augmented system actuation matrix is full rank, allowing the desired virtual inputs for step I of the steering algorithm to be generated as

$$v = \left[g_1(\gamma(t)) \ \cdots \ g_{m+p}(\gamma(t)) \right]^{-1} \dot{\gamma}(t) \tag{22}$$

Once we have the desired virtual inputs via (22), they must be mapped to the original system inputs $u \in \mathbb{R}^m$ for motion generation. This is challenging because the virtual inputs related to the Lie brackets $v_{m+1}, ..., v_{m+p}$ are realized by sequentially switching the actual inputs u, causing interference with the first m vector fields.

This issue, addressed in Lafferriere and Sussmann (1991), associates our inputs with a suitable choice of time functions related to virtual inputs and the Philip Hall basis vector fields g_i, $i = 1, ..., m + p$. So, the Chen-Fliess series characterizing our nonlinear system can be written as

$$S_t(X) = e^{z_{m+p} g_{m+p}} e^{z_{m+p-1} g_{m+p-1}} \cdots e^{z_2 g_2} e^{z_1 g_1}(X) \tag{23}$$

Here, e^{tg_i} denotes the *formal exponential* of g_i, representing the flow associated with the solution of the differential equation $\dot{X} = g_i(X)$ at time t starting from X at time 0. The variables $z_1, ..., z_{m+p}$ are functions of time and are called the backward Philip Hall coordinates. They are related to the amount of time that the system must flow along each vector field to generate the desired motion. The exponential terms can be expanded using the identity

$$e^{tg_i} = I + tg_i + \tfrac{1}{2}t^2[g_i]^2 + \tfrac{1}{6}t^3[g_i]^3 + \cdots \tag{24}$$

where the vector field powers are to be defined with respect to Lie bracketing operations. Given (20), the Chen-Fliess series satisfies the following relationship

$$\dot{S}(t) = S(t)(g_1 v_1 + g_2 v_2 + ... + g_{m+p} v_{m+p}), \quad S(0) = I \tag{25}$$

To solve for the backward Philip Hall coordinates in terms of the virtual input v, we differentiate (23) directly, using (24) to write the expansion for a sufficiently high order of terms to capture all Philip Hall basis, and equating to (25). This yields the following ordinary differential equations

$$\dot{z} = Q(z)v, \quad z(0) = 0 \tag{26}$$

Determining real inputs is simpler with the forward Philip Hall coordinates. The following equation shows a formal system with forward Philip Hall coordinates, where we highlight the difference in the order of the applied flows as compared to (23)

$$S_t(X) = e^{\bar{z}_1(t) g_1} e^{\bar{z}_2(t) g_2} \cdots e^{\bar{z}_{m+p}(t) g_{m+p}}(X) \tag{27}$$

By relating (27) to (23) via an algebraic transformation, one can establish a relationship between the backward and forward Philip Hall coordinates by the following equation

$$e^{z_{m+p}(t) g_{m+p}} \cdots e^{z_1(t) g_1}(q_0) = e^{\bar{z}_1(t) g_1} \cdots e^{\bar{z}_{m+p}(t) g_{m+p}}(q_0) \tag{28}$$

4.2 Motion Generation Along Vector Fields

The derivation of the forward Philip Hall coordinates almost completes the second step of the steering algorithm as they impart information regarding how long we need to let the dynamical system flow along each of the vector fields ($g_1, g_2, [g_1, g_2]$ in our case). Since g_1 and g_2 are the vector fields belonging to the non-extended dynamical system (5), we can set the input $u_1 = 1$ for $\bar{z}_1$ seconds to achieve the flow along $e^{\bar{z}_1 g_1}$. Similarly, we can set the input $u_2 = 1$ for $\bar{z}_2$ seconds to achieve a flow along $e^{\bar{z}_2 g_2}$. The following sequential switching generates the flow along $e^{\bar{z}_3 g_3}$ or, equivalently, $e^{\bar{z}_3 [g_1, g_2]}$: (1) Set $u_1 = 1$, $u_2 = 0$ for $t \in [0, \sqrt{\bar{z}_3}]$, (2) Set $u_1 = 0$, $u_2 = 1$ for $t \in [\sqrt{\bar{z}_3}, 2\sqrt{\bar{z}_3}]$, (3) Set $u_1 = -1$, $u_2 = 0$ for $t \in [2\sqrt{\bar{z}_3}, 3\sqrt{\bar{z}_3}]$, (4) Set $u_1 = 0$, $u_2 = -1$ for $t \in [3\sqrt{\bar{z}_3}, 4\sqrt{\bar{z}_3}]$. The input magnitude can vary as long as its consistent across vector fields.

As Lafferriere and Sussmann (1991) shows, the sequential switching yields $e^{\bar{z}_3 [g_1, g_2]}$ exactly only if the system's order of nilpotency is 2, meaning all the Lie brackets of order 3 and higher are zero. For systems with nilpotentcy greater than 2, which is the case for our particular magnetic system, the sequential switching only gives rise to $e^{\bar{z}_3 [g_1, g_2]}$ "approximately", since it actually gives rise to

$$e^{\bar{z}_3 [g_1, g_2]} e^{\gamma [g_1, [g_1, g_2]]} e^{-\gamma [g_2, [g_1, g_2]]}$$

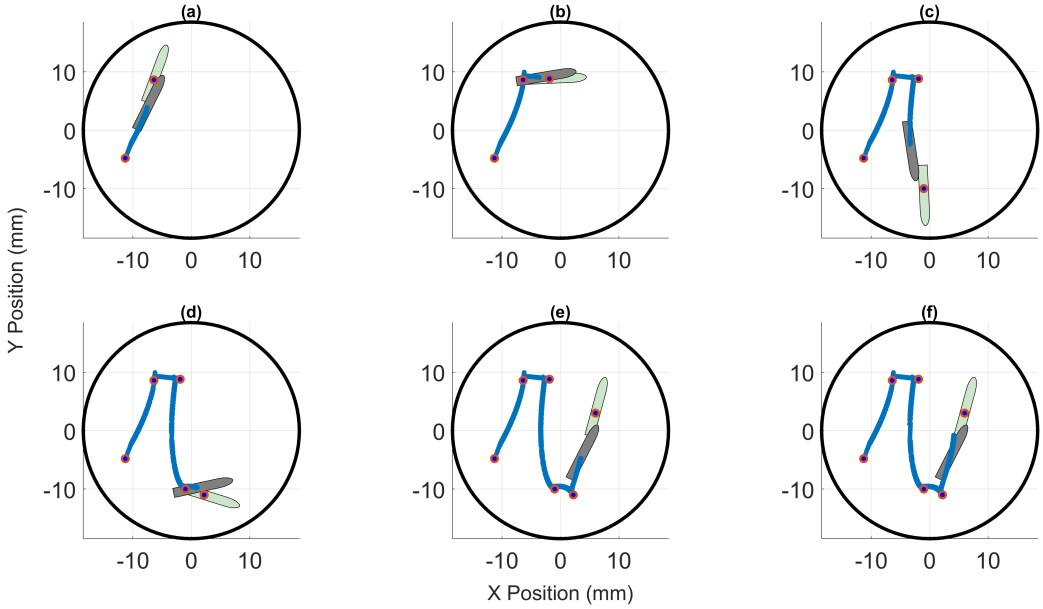

Fig. 2. The grey patch represents a magnetic needle (radius 0.8mm, length 8mm), while the green patch shows the next waypoint and desired orientation. Initial position: (-11.3 mm, -4.8 mm). Initial orientation: 69.9 deg. Snapshots are at (a) T=200s, (b) T=440s, (c) T=650s, (d) T=1020s, (e) T=1220s, (f) T=1300s.

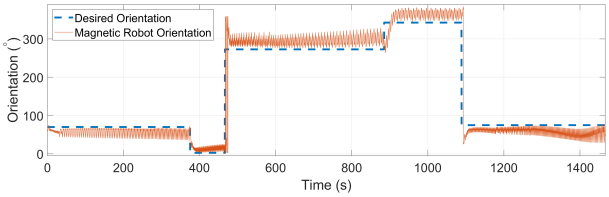

Fig. 3. Comparison of achieved vs. desired magnetic robot orientation for the entire suturing path.

where $\gamma = \frac{1}{2}\bar{z}_3^{\frac{3}{2}}$. For small values of $\bar{z}_3$, higher order brackets can be neglected. However, this approach yields approximate (as opposed to exact) tracking.

5. SIMULATION RESULTS

We use MATLAB R2021a to simulate a magnetic needle's motion in a plane as shown in Fig. 1. We deploy the steering algorithm described in Section 4 for waypoint tracking. The reference path is given by linear interpolation of the waypoints, which are selected to be representative of a suturing path that is common for surgical procedures such as hernia repair. The 6 waypoints' coordinates (in mm) starting from the leftmost waypoint are (-11.3, -4.8), (-6.4, 8.6), (-1.9, 8.8), (-1, -10), (2.2, -11) and (6, 3). The desired magnetic robot heading is always aligned with the vector from previous waypoint to the next one. Fig. 2 provides snapshots of the surgical needle along different times during the execution. Fig. 3 shows the orientation throughout execution. The Euclidean RMS errors for each of the five segments of the suturing path are 0.41 mm, 0.49 mm, 1.53 mm, 0.67 mm and 1.01 mm, respectively. The average Euclidean RMS error for the path is 0.82 mm.

6. CONCLUSIONS

This paper applies Chow's Theorem to magnetic robotic systems, exploring the nonlinearity of magnetic fields to enable motion that standard control techniques might deem infeasible. We offer a simple condition to assess motion feasibility for a single magnetic tool powered by arbitrary number of electromagnets and apply it to an underactuated case. Furthermore, we provide a framework to compute the degree of nonholonomy of such a system which can be extended to a 6-DOF underactuated system. Once the motion feasibility study reveals the complexity of motion required to make the robot move in the workspace (directly linked with the order of Lie brackets that need to be computed), we deploy a steering algorithm which can steer the robot between any two points in the workspace without encountering actuation matrix inversion singularities with low tracking error. Due to the non-nilpotent nature of magnetic fields, this steering is approximate. Future work will focus on synthesizing controllers that would compensate for the non-nilpotency and enhance tracking performance.

REFERENCES

Abbott, J.J., Diller, E., and Petruska, A.J. (2020). Magnetic methods in robotics. *Annual Review of Control, Robotics, and Autonomous Systems*, 3, 57–90.

Antoniou, S.A., Pointner, R., and Granderath, F.A. (2011). Single-incision laparoscopic cholecystectomy: a systematic review. *Surgical endoscopy*, 25, 367–377.

Bao, Z.F. and Diller, E. (2022). Evaluating miniature robot surgical scissors. In *2022 International Conference on Manipulation, Automation and Robotics at Small Scales (MARSS)*, 1–6.

Chamberlain, R.S. and Sakpal, S.V. (2009). A comprehensive review of single-incision laparoscopic surgery (sils) and natural orifice transluminal endoscopic surgery (notes) techniques for cholecystectomy. *Journal of Gastrointestinal Surgery*, 13(9), 1733–1740.

Dreyfus, R., Boehler, Q., Lyttle, S., Gruber, P., Lussi, J., Chautems, C., Gervasoni, S., Berberat, J., Seibold, D., Ochsenbein-Kölble, N., et al. (2024). Dexterous

helical magnetic robot for improved endovascular access. *Science Robotics*, 9(87), eadh0298.

Erin, O., Liu, X., Ge, J., Opfermann, J., Barnoy, Y., Mair, L.O., Kang, J.U., Gensheimer, W., Weinberg, I.N., Diaz-Mercado, Y., et al. (2022a). Overcoming the force limitations of magnetic robotic surgery: Magnetic pulse actuated collisions for tissue-penetrating-needle for tetherless interventions. *Adv. Intell. Syst.*, 4(6), 2200072.

Erin, O., Raval, S., Schwehr, T.J., Pryor, W., Barnoy, Y., Bell, A., Liu, X., Mair, L.O., Weinberg, I.N., Krieger, A., and Diaz-Mercado, Y. (2022b). Enhanced accuracy in magnetic actuation: Closed-loop control of a magnetic agent with low-error numerical magnetic model estimation. *IEEE Robotics and Automation Letters*, 7(4), 9429–9436. doi:10.1109/LRA.2022.3191047.

Fruchard, M. (2023). Controllability and control synthesis of underactuated magnetic microrobots. *Automatica*, 149, 110823.

Kummer, M.P., Abbott, J.J., Kratochvil, B.E., Borer, R., Sengul, A., and Nelson, B.J. (2010). Octomag: An electromagnetic system for 5-dof wireless micromanipulation. *IEEE Trans. Rob.*, 26(6), 1006–1017.

Kuntz, A., Emerson, M., Ertop, T.E., Fried, I., Fu, M., Hoelscher, J., Rox, M., Akulian, J., Gillaspie, E.A., Lee, Y.Z., et al. (2023). Autonomous medical needle steering in vivo. *Science Robotics*, 8(82), eadf7614.

Lafferriere, G. and Sussmann, H. (1991). Motion planning for controllable systems without drift. In *Proceedings. 1991 IEEE International Conference on Robotics and Automation*, 1148–1149. IEEE Computer Society.

Maeso, S., Reza, M., Mayol, J.A., Blasco, J.A., Guerra, M., Andradas, E., and Plana, M.N. (2010). Efficacy of the da vinci surgical system in abdominal surgery compared with that of laparoscopy: a systematic review and meta-analysis. *Annals of surgery*, 252(2), 254–262.

Mair, L.O., Liu, X., Dandamudi, B., Jain, K., Chowdhury, S., Weed, J., Diaz-Mercado, Y., Weinberg, I.N., and Krieger, A. (2020). Magnetosuture: Tetherless manipulation of suture needles. *IEEE Trans. Med. Rob. Bionics*, 2(2), 206–215.

Nguyen, K.T., Hoang, M.C., Go, G., Kang, B., Choi, E., Park, J.O., and Kim, C.S. (2020). Regularization-based independent control of an external electromagnetic actuator to avoid singularity in the spatial manipulation of a microrobot. *Control Engineering Practice*, 97, 104340. doi:https://doi.org/10.1016/j.conengprac.2020.104340. URL `https://www.sciencedirect.com/science/article/pii/S0967066120300265`.

Ongaro, F., Pane, S., Scheggi, S., and Misra, S. (2018). Design of an electromagnetic setup for independent three-dimensional control of pairs of identical and nonidentical microrobots. *IEEE Trans. Rob.*, 35(1), 174–183.

Petruska, A.J. and Nelson, B.J. (2015a). Minimum bounds on the number of electromagnets required for remote magnetic manipulation. *IEEE Trans. Rob.*, 31(3), 714–722.

Petruska, A.J. and Nelson, B.J. (2015b). Minimum bounds on the number of electromagnets required for remote magnetic manipulation. *IEEE Transactions on Robotics*, 31(3), 714–722. doi:10.1109/TRO.2015.2424051.

Raval, S., Erin, O., Liu, X., Mair, L.O., Pryor, W., Barnoy, Y., Weinberg, I.N., Krieger, A., and Diaz-Mercado, Y. (2021). Magnetic model calibration for tetherless surgical needle manipulation using zernike polynomial fitting. In *2021 IEEE 21st International Conference on Bioinformatics and Bioengineering (BIBE)*, 1–6. doi:10.1109/BIBE52308.2021.9635512.

Raval, S., Mair, L., Pryor, W., Erin, O., Schwehr, T., Budaraju, J., Krieger, A., and Diaz-Mercado, Y. (2023). Time-scale separation analysis for surgical needle control in electromagnetic robotic systems. *IFAC-PapersOnLine*, 56(3), 307–312. doi:https://doi.org/10.1016/j.ifacol.2023.12.042. URL `https://www.sciencedirect.com/science/article/pii/S2405896323023753`. 3rd Modeling, Estimation and Control Conference MECC 2023.

Saeidi, H., Opfermann, J.D., Kam, M., Wei, S., Léonard, S., Hsieh, M.H., Kang, J.U., and Krieger, A. (2022). Autonomous robotic laparoscopic surgery for intestinal anastomosis. *Science Robotics*, 7(62), eabj2908.

Salehizadeh, M. and Diller, E. (2016). Two-agent formation control of magnetic microrobots. In *2016 International Conference on Manipulation, Automation and Robotics at Small Scales (MARSS)*, 1–6. IEEE.

Salehizadeh, M. and Diller, E.D. (2021). Path planning and tracking for an underactuated two-microrobot system. *IEEE robotics and automation letters*, 6(2), 2674–2681.

Sastry, S. (2013). *Nonlinear systems: analysis, stability, and control*, volume 10. Springer Science & Business Media.

Wang, T., Ugurlu, H., Yan, Y., Li, M., Li, M., Wild, A.M., Yildiz, E., Schneider, M., Sheehan, D., Hu, W., et al. (2022). Adaptive wireless millirobotic locomotion into distal vasculature. *Nature Communications*, 13(1), 4465.

Zhang, J., Onaizah, O., Middleton, K., You, L., and Diller, E. (2017). Reliable grasping of three-dimensional untethered mobile magnetic microgripper for autonomous pick-and-place. *IEEE Robotics and Automation Letters*, 2(2), 835–840.

Zhao, H., Leclerc, J., Feucht, M., Bailey, O., and Becker, A.T. (2020). 3d path-following using mrac on a millimeter-scale spiral-type magnetic robot. *IEEE Robotics and Automation Letters*, 5(2), 1564–1571. doi:10.1109/LRA.2020.2969159.

Appendix A. THE DIPOLE MODEL

This section provides equation for computing $\bar{B}_k$ from k^{th} coil using a dipole model, used in our simulations. Let $d_k(x) = x - r_k$ be a vector from the k^{th} coil center $r_k \in \mathbb{R}^2$ to the point of interest $x \in \mathcal{W} \subset \mathbb{R}^2$. Let $m_k \in \mathbb{R}^2$ be the dipole moment of the coil.

$$\bar{B}_k(x) = \frac{m_k}{4\pi\|d_k(x)\|^3} - \frac{3d_k(x)m_k^T d_k(x)}{4\pi\|d_k(x)\|^5} \tag{A.1}$$

$$\nabla\bar{B}_k(x) = \frac{15d_k(x)d_k(x)^T m_k d_k(x)^T}{4\pi\|d_k(x)\|^7} - \frac{3m_k d_k(x)^T + 3d_k(x)m_k^T + 3(m_k^T d_k(x))I}{4\pi\|d_k(x)\|^5} \tag{A.2}$$